Investigation of Strain-Temperature Cross-Sensitivity of FBG Strain Sensors Embedded Onto Different Substrates

Heying QIN[1,2,3], Pengfei TANG[1,2,3], Jing LEI[1,2,3], Hongbin CHEN[1,2,3], and Boguang LUO[1,2,3*]

[1]*Collaborative Innovation Center for Exploration of Hidden Nonferrous Metal Deposits and Development of New Materials in Guangxi, Guilin University of Technology, Guilin 541004, China*

[2]*Guangxi Engineering Research Center of Intelligent Structural Material, Guilin University of Technology, Guilin 541004, China*

[3]*Guangxi Key Laboratory of Geotechnical Mechanics and Engineering, Guilin University of Technology, Guilin 541004, China*

[*]Corresponding author: Boguang LUO E-mail: luoboguang@126.com

Abstract: The strain-temperature cross-sensitivity problem easily occurs in the engineering strain monitoring of the self-sensing embedded with fiber Bragg grating (FBG) sensors. In this work, a theoretical investigation of the strain-temperature cross-sensitivity has been performed using the temperature reference grating method. To experimentally observe and theoretically verify the problem, the substrate materials, the preloading technique, and the FBG initial central wavelength were taken as main parameters. And a series of sensitivity coefficients calibration tests and temperature compensation tests have been designed and carried out. It was found that when the FBG sensors were embedded on different substrates, their coefficients of the temperature sensitivity were significantly changed. Besides, the larger the coefficients of thermal expansion (CTE) of substrates were, the higher the temperature sensitivity coefficients would be. On the other hand, the effect of the preloading technique and FBG initial wavelength was negligible on both the strain monitoring and temperature compensation. In the case of similar substrates, we did not observe any difference between temperature sensitivity coefficients of the temperature compensation FBG with one free end or two free ends. The curves of the force along with temperature were almost overlapped with minor differences (less than 1%) gained by FBG sensors and pressure sensors, which verified the accuracy of the temperature compensation method. We suggest that this work can provide efficient solutions to the strain-temperature cross-sensitivity for engineering strain monitoring with the self-sensing element embedded with FBG sensors.

Keywords: FBG sensor; self-sensing element embedded FBG sensor; cross sensitivity of strain and temperature; temperature compensation

Citation: Heying QIN, Pengfei TANG, Jing LEI, Hongbin CHEN, and Boguang LUO, "Investigation of Strain-Temperature Cross-Sensitivity of FBG Strain Sensors Embedded Onto Different Substrates," *Photonic Sensors*, 2023, 13(1): 230127.

1. Introduction

Steel strands, carbon fiber reinforcement, and fiberglass reinforcement are the key materials that have stressed elements in the engineering structure. For example, bridge cables/suspenders/hangers,

Received: 24 January 2022 / Revised: 26 May 2022

DOI: 10.1007/s13320-022-0668-3
Article type: Regular

anchor cables of side/protecting slopes, and prestressed members of large-span structures are mostly consisting of these high-strength materials. However, the failure probability of stressed components has been increased day by day due to coupling corrosion, caused by multi-factors such as environment, temperature, and high stress when they are in use [1–5]. Thus, the safety monitoring of these key materials is a very crucial means to prevent accidents in this engineering structure [6–9]. So far, many national and internal researchers have applied a variety of structural health monitoring methods for practical engineering [10–13]. Among these methods, the civil engineering monitoring technology using FBG sensors is more mature [14–16]. Yet, the fiber Bragg grating (FBG) can be easily affected by temperature variation, caused by day-and-night, season, interior-and-exterior, and partial heating-and-cooling, which are responsible for strain-temperature cross-sensitivity. Shiratsuchi *et al.* [17] have investigated and developed a new type of the FBG strain sensor with the temperature compensation pre-tensioning package under low temperatures. They have successfully eliminated the transverse effects and strain errors of FBG strain sensors which were directly pasted on the monitored structure. Wang *et al.* [18] elevated the accuracy of the temperature compensation using the double gratings method. Besides, Wang *et al.* [19] reported a symmetrical push-pull structure that had efficiently removed the effect of temperature on the wavelength changes and achieved excellent performance. Iwashima *et al.* [20] utilized the packaging FBG technique with liquid crystalline polymer tubes and reduced the temperature sensitivity from 1 nm/100 ℃ to 0.13 nm/100 ℃. Moreover, there are lots of reports on the strain-temperature cross-sensitivity as well [21–24]. In order to solve the strain-temperature cross-sensitivity problem, different methods must be applied to various types of FBG sensors. We have applied an embedded preloading technique to FBG sensors and enhanced the monitoring range. Our self-sensing element embedded FBG technology has achieved material's self-monitoring in the process of being stressed [25]. Meanwhile, fatigue performance [26], corrosion resistance property, and life prediction [27] were systematically investigated. This technology was applied to make the self-sensing steel strands embedding FBG sensor which was used for the health monitoring of internal and external losses of pre-stress, cables, rock, and soil anchor cables [28, 29]. The change in temperature affected not only the embedded FBG wavelength variation but also the internal forces of the components (stress and strain) owing to the structures being hyperstatic. So, the effect of temperature on the central wavelength of the FBG sensor should be eliminated when we calculated the internal forces of the structure. That is the way to solve the FBG strain-temperature cross-sensitivity problem. Herein, a series of tests have been performed to solve the strain-temperature cross-sensitivity problem of the FBG strain sensors embedded onto different substrates. Theoretical and experimental observations of this problem were systematically conducted based on the prime parameters such as substrate materials, the preloading technique, and the FBG initial central wavelength. Finally, the effective solutions were put forward to deal with the problem of strain-temperature cross-sensitivity to monitor the engineering strain.

2. Strain and temperature cross-sensitivity and temperature compensation principle of the FBG strain sensor

According to the coupled-mode theory, the characteristic equation for the FBG is $\lambda_B = 2n_{\text{eff}}\Lambda$, where the central wavelength λ_B is positively correlated to its periods and the refractive index of the fiber core. When an outside physical quantity is sensed by the FBG, it changes the refractive index n_{eff} and period Λ, and the corresponding central wavelength will vary. The equation for $\Delta\lambda$

(variation of FBG's central wavelength) is as following:

$$\frac{\Delta\lambda_B}{\lambda_B}=\frac{\Delta\Lambda}{\Lambda}+\frac{\Delta n_{\text{eff}}}{n_{\text{eff}}}. \quad (1)$$

In the case of the FBG sensor for monitoring civil engineering, the central wavelength of the FBG varies due to two factors – strain and temperature, and there is usually a cross-sensitivity between them. The influences of strain and temperature on the FBG central wavelength are theoretically analyzed in the following three conditions.

2.1 Bare fiber Bragg grating without the coupling substrate

When a bare FBG (without the coupling substrate) is subjected to the strain and temperature at the same time, its axial strain will change the periods, and the elasto-optical effect changes the refractive index of the fiber core. Thermal expansion of temperature variation causes differences in FBG periods, while the thermal-optical effect changes the FBG effective refractive index. Under these conditions, the drifting value of the FBG central wavelength is

$$\Delta\lambda_B=(1-P_e)\lambda_B\varepsilon_x+\left(\xi_F+\alpha_F\right)\lambda_B\Delta T. \quad (2)$$

When the strain sensitivity coefficients of the bare FBG is $K_{\varepsilon-F}=(1-P_e)\lambda_B$, the temperature sensitivity coefficient is $K_{T-F}=(\xi_F-\alpha_F)\lambda_B$. Then, it can be simplified as

$$\Delta\lambda_B=K_{\varepsilon-F}\varepsilon_x+K_{T-F}\Delta T \quad (3)$$

where P_e is the valid elastic-optic coefficient. In the case of common silica fibers, its value is kept as 0.22. ξ_F is the thermal-optic coefficient of fibers and α_F is the fiber CTE (the coefficients of thermal expansion), which is valued at $\xi_F=6.55\times10^{-6}$ and $\alpha_F=0.55\times10^{-6}$, respectively.

2.2 Effect of temperature on the fiber Bragg grating embedded on the substrate

When the CTE of substrate materials α_M is different from the CTE of the FBG α_F, the FBG embedded onto the substrate is subjected to the stress which is caused by the temperature variations of subtracting materials. As described in [30], this force is due to different coefficients of thermal expansion and can be approximated as the axial force, where the axial strain of the FBG is $\varepsilon_x=(\alpha_M-\alpha_F)\Delta T$. This axial strain is in accord with the fact that the bare FBG is influenced by both strain and temperature. As shown in (4):

$$\Delta\lambda_B=[(1-P_e)(\alpha_M-\alpha_F)+(\xi_F+\alpha_F)]\lambda_B\Delta T=K_{T-M}\Delta T \quad (4)$$

where $K_{T-M}=[(1-P_e)(\alpha_M-\alpha_F)+(\xi_F+\alpha_F)]\lambda_B$ is the temperature sensitivity coefficient of the FBG embedded onto substrates. Compared with (3) and (4), when the bare FBG and the embedded FBG are subjected to the temperature variations, the difference in temperature sensitivity coefficients between them is calculated with the help of (5):

$$K_{T-M}-K_{T-F}=(1-P_e)(\alpha_M-\alpha_F)\Delta\lambda_B. \quad (5)$$

As shown in (5), if the CTE of the substrate is larger than that of the FBG, $K_{T-M}-K_{T-F}>0$, the FBG would be subjected to the tensile strength along with an increase in the temperature. On the other hand, if it is lower, the FBG would be subjected to the pressure.

2.3 Effect of temperature and axial strain on the fiber Bragg grating embedded onto the substrate and the principle of temperature compensation

Based on the analysis of Sections 1.1 and 1.2, the variations in the central wavelength of the FBG embedded onto substrates are affected by both the temperature and axial strain, and can be calculated as

$$\begin{aligned}\Delta\lambda_B&=(1-P_e)\lambda_B\varepsilon_x+\left[\left(1-P_e\right)\left(\alpha_M-\alpha_F\right)+\left(\xi_F+\alpha_F\right)\right]\lambda_B\Delta T\\&=K_{\varepsilon-M}\varepsilon_x+K_{T-M}\Delta T.\end{aligned} \quad (6)$$

Equation (6) is the principle of monitoring stress or strain by the FBG in civil engineering. When the coupling components of the FGB are subjected to the stress and temperature variations, the variations of the FBG central wavelength should clarify how many variations are caused by the temperature and how many variations are caused by the external axial strain.

According to (6), $K_{\varepsilon-M}=(1-P_e)\lambda_B$ and $K_{T-M}=[(1-P_e)(\alpha_M-\alpha_F)+(\xi_F+\alpha_F)]\lambda_B$ could be obtained from the calibration of the sensor and ΔT could be obtained from the unstressed FBG sensor, namely temperature compensation sensor. Using (4): $\Delta T=\dfrac{\Delta\lambda_C}{K_{T-M-C}}$, the strain produced from the stressed components is monitored by the FBG strain sensor and can be calculated by putting (4) into (6):

$$\varepsilon=\frac{\Delta\lambda_s-\dfrac{K_{T-M-S}}{K_{T-M-C}}\Delta\lambda_C}{K_{\varepsilon-M-S}} \tag{7}$$

where ε is the obtained strain of stressed components; $\Delta\lambda_s$ and $\Delta\lambda_C$ are respectively the variations of the central wavelength of the FBG strain sensor which are influenced by the stress and temperature variations (namely the strain FBG sensor, hereafter). Moreover, the temperature compensation sensor is only affected by the temperature (namely the temperature compensation FBG sensor, hereafter); K_{T-M-S} and K_{T-M-C} are the temperature sensitivity coefficients of the strain FBG sensor and the temperature compensation FBG sensor; $K_{\varepsilon-M-S}$ is the strain sensitivity coefficients of the strain FBG sensor. All of these coefficients could be obtained from the calibration. In (7), the strain-temperature cross-sensitivity is addressed by embedding an unstressed (free) FBG temperature sensor. Besides, the partial variations of the strain sensor's central wavelength variations are obtained which are caused by the temperature variations. And the change in the central wavelength caused by the stress can be gained, which is the temperature compensation principle of the temperature reference grating method.

3. Experimental study

FBG sensors were used in the strain monitoring of civil engineering and could be subjected to the stress and the temperature differences among seasons, day and night, and above and below the ground. To accurately determine the strain of components, the temperature compensation should be conducted on the FBG sensors. This could be processed as (7). In order to accurately simulate the components that were affected by both the stress and temperature differences in actual engineering, special experimental facilities were developed. In this work, we have designed a systematic experimental plan to precisely measure the sensitivity coefficients.

3.1 Experimental specimen

To further investigate the strain-temperature cross-sensitivity of FBG sensors in different substrates, three substrate materials with different CTEs were selected such as steel wires (central wire of steel strand), carbon fiber reinforcement, and fiberglass reinforcement. The basic parameters of specimen substrate materials are shown in Table 1.

Table 1 Relevant properties of substrate materials.

Types of base	Sectional area (mm^2)	Tensile strength (MPa)	Elastic modulus (GPa)	Density (kg/m^3)	Linear expansion coefficient (nm/℃)
Steel wire	21.23	1860	195	7850	11.96×10^{-6}
Carbon fiber reinforcement	28.26	2200	140	1600	7.09×10^{-6}
Fiberglass reinforcement	28.26	610	40	1300	5×10^{-6}

Qin *et al.* [25] used a set of longitudinal grooves on the central wire with the depth and width of 0.4 mm and 1 mm, respectively. When the central wire was loaded and tensioned, the FBG was stuck and embedded in the groove and pasted with epoxy resin. The embedded preloading process has achieved good results in expanding the monitoring range of the FBG strain sensor. The test components and cross-sections made by the embedded preloading process are shown in Fig. 1.

For investigating the strain-temperature cross-sensitivity performance of FBG sensors of the preloading technique, two coupling modes of the strain FBG sensor were devised in this work, which were groove preloading and groove non-preloading. These were adopted in the test specimen. The specific coupling modes and processes are shown in

[25], while the design of the specimen is listed in Table 2.

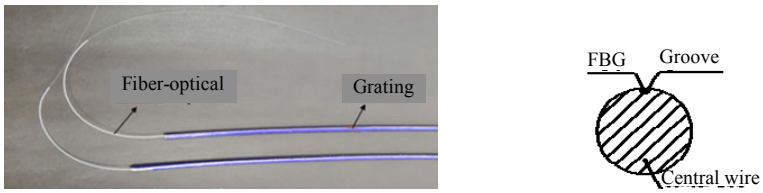

(a) (b)

Fig. 1 Schematic diagram of the test piece: (a) embedded preloading process and (b) cross-section diagram of the central wire.

Table 2 Experimental specimen.

Specimen number	Substrate material	FBG coupling mode	Temperature compensation FBG number	Central wavelength of temperature compensation FBG (nm)	Strain FBG number	Central wavelength of strain FBG(nm)
SW-A1	Steel wire	Preloading	$FBG_{SW-A1-C}$	1532	$FBG_{SW-A1-S}$	1532
SW-A2	Steel wire	Preloading	$FBG_{SW-A2-C}$	1540	$FBG_{SW-A2-S}$	1540
SW-A3	Steel wire	Preloading	$FBG_{SW-A3-C}$	1548	$FBG_{SW-A3-S}$	1548
SW-B1	Steel wire	Non preloading	$FBG_{SW-B1-C}$	1532	$FBG_{SW-B1-S}$	1532
SW-B2	Steel wire	Non preloading	$FBG_{SW-B2-C}$	1540	$FBG_{SW-B2-S}$	1540
SW-B3	Steel wire	Non preloading	$FBG_{SW-B3-C}$	1548	$FBG_{SW-B3-S}$	1548
CFRP-A1	Carbon fiber reinforcement	Preloading	$FBG_{CFRP-A1-C}$	1532	$FBG_{CFRP-A1-S}$	1532
CFRP-A2	Carbon fiber reinforcement	Preloading	$FBG_{CFRP-A2-C}$	1540	$FBG_{CFRP-A2-S}$	1540
CFRP-A3	Carbon fiber reinforcement	Preloading	$FBG_{CFRP-A3-C}$	1548	$FBG_{CFRP-A3-S}$	1548
CFRP-B1	Carbon fiber reinforcement	Non preloading	$FBG_{CFRP-B1-C}$	1532	$FBG_{CFRP-B1-S}$	1532
CFRP-B2	Carbon fiber reinforcement	Non preloading	$FBG_{CFRP-B2-C}$	1540	$FBG_{CFRP-B2-S}$	1540
CFRP-B3	Carbon fiber reinforcement	Non preloading	$FBG_{CFRP-B3-C}$	1548	$FBG_{CFRP-B3-S}$	1548
FGRP-A1	Fiberglass reinforcement	Preloading	$FBG_{FGRP-A1-C}$	1532	$FBG_{FGRP-A1-S}$	1532
FGRP-A2	Fiberglass reinforcement	Preloading	$FBG_{FGRP-A2-C}$	1540	$FBG_{FGRP-A2-S}$	1540
FGRP-A3	Fiberglass reinforcement	Preloading	$FBG_{FGRP-A3-C}$	1548	$FBG_{FGRP-A3-S}$	1548
FGRP-B1	Fiberglass reinforcement	Non preloading	$FBG_{FGRP-B1-C}$	1532	$FBG_{FGRP-B1-S}$	1532
FGRP-B2	Fiberglass reinforcement	Non preloading	$FBG_{FGRP-B2-C}$	1540	$FBG_{FGRP-B2-S}$	1540
FGRP-B3	Fiberglass reinforcement	Non preloading	$FBG_{FGRP-B3-C}$	1548	$FBG_{FGRP-B3-S}$	1548

Notes: For the specimen number, the letters before "-" represent the type of the substrate, where SW is the steel wire, CFRP denotes the carbon fiber reinforcement, and FGRP represents the fiberglass reinforcement; the letters after "-" represent the coupling modes between the FBG and substrate materials, where A is the preloading and B is the non-preloading; the last number represents the initial central wavelength of the FBG, in which 1 is the initial wavelength of 1532 nm, 2 is the initial wavelength of 1540 nm, and 3 is the initial wavelength of 1548 nm. For one specimen, the central wavelength of the temperature compensation FBG is kept the same as that of the strain FBG.

3.2 Temperature sensitivity coefficient test

In the case of the bare FBG, its temperature sensitivity coefficient K_{T-F} was measured with the help of the water bath method [31]. To conduct the water bath experiment at a constant temperature, the FBG was immersed in the beaker and filled with water. In this case, the initial temperature was set to 30 ℃ and increased up to 100 ℃ with 10 ℃ per

step. When the temperature at each step became stable, the central wavelength of the FBG was collected.

The temperature sensitivity coefficient K_{T-M} of the FBG sensors with coupling substrates was measured when the specimen with coupling FBG sensors was free at two ends. The test heating device is shown in Fig. 2. To realize the temperature variations, the water in the quartz glass tube was heated by an alcohol burner, as shown in Fig. 2. Considering the length of a substrate and even heating, four alcohol burners were evenly placed along the glass tube between silicone plugs. The test specimen and temperature gauge were inserted into the quartz glass tube and the two ends of the glass tube, filled with water, were sealed. The temperature variations during heating were recorded with the help of a temperature gauge, where the initial temperature was set to 3 ℃ and increased up to 100 ℃ with 10 ℃ per step. The central wavelength of the FBG was collected when the temperature at each step became stable. In this paper, the Agilent 86142b demodulator was used to collect the wavelength of the FBG. The wavelength range of the demodulator was 1525 nm – 1570 nm, the sampling frequency was 1Hz, the wavelength accuracy was 2.5 pm, and the resolution was 1 pm.

Linear fitting was made with temperature as the abscissa and variations of the FBG central wavelength $\Delta\lambda_B$ as the ordinate and the resulting slope of the fitting straight line was temperature sensitivity of the FBG sensors, K_{T-F} or K_{T-M}. As shown in Fig. 3, the fitting of temperature sensitivity coefficients of the FBG sensors, embedded in the steel wire before and after coupling, was taken as an example.

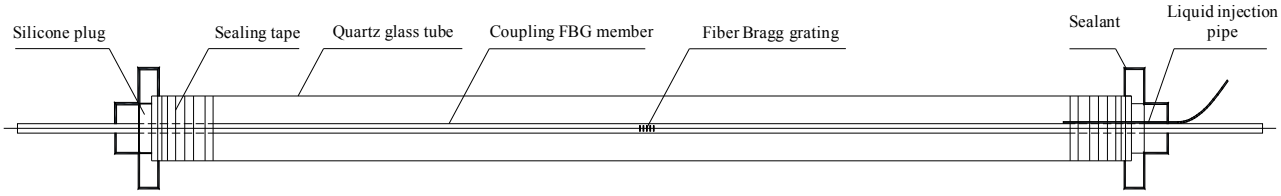

Fig. 2 Schematic diagram of the test heating device.

From Fig. 3, it is analyzed that the variations of the FBG central wavelength $\Delta\lambda_B$ and the temperature *T* have a good linear relationship with a correlation coefficient above 99.99%. The more the improvement of temperature is, the larger the $\Delta\lambda_B$ will be, which is also consistent with the theory. The comparative theoretical value of the temperature sensitivity coefficient of the bare optical fiber $K_{T-F}=(\xi_F+\alpha_F)\lambda_B$ and the theoretical value of the temperature sensitivity coefficient of the embedded substrate material $K_{T-M}=[(1-P_e)(\alpha_M-\alpha_F)+(\xi_F+\alpha_F)]\lambda_B$ with their test values are listed in Table 3.

Comparative analysis of the data in Table 3 leads us to conclude that the experimental and theoretical values of temperature sensitivity coefficients K_{T-F} of the bare FBG and temperature sensitivity coefficients K_{T-M} of the FBG sensor with coupling substrates have little error rate (less than 3%). The temperature sensitivity coefficients K_{T-M} of the FBG sensors in three different substrates have a large difference, indicating that the effects of the substrate material on temperature sensitivity coefficients are directly related to the temperature expansion coefficient of the substrate. The larger expansion coefficient of the substrate is responsible for the larger temperature sensitivity coefficients, which is also consistent with the theoretical formula. In the case of three substrate materials, as the temperature expansion coefficient of steel wire is the largest, K_{T-M} of the steel wire is also the highest. This is followed by K_{T-M} of the carbon fiber substrate and that of the fiberglass substrate is the lowest.

The experimental and theoretical values difference $K_{T-M} - K_{T-F}$ of these three substrate materials exhibit a little error rate of less than 3%. On the other hand, when the FBG has the same initial wavelength, K_{T-F} values of Group A (preloading in making FBG) and Group B (non-preloading in making FBG) show a little difference. Therefore, the temperature expansion coefficient of the substrate is the major factor that influences K_{T-M}.

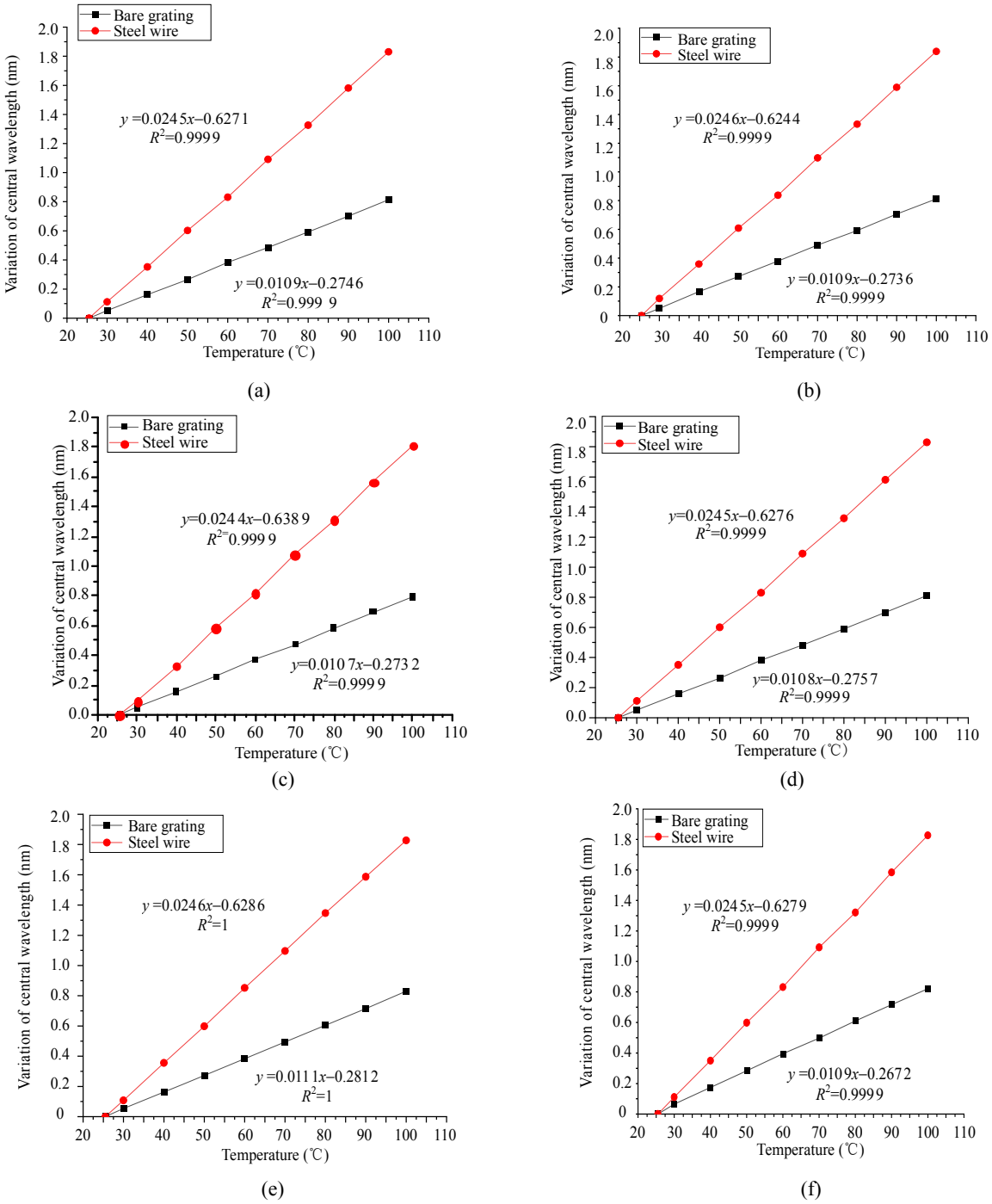

Fig. 3 K_{T-F} and K_{T-M} of the FBG sensor embedded in the steel wire: (a) $FBG_{GS-A1-C}$, (b) $FBG_{GS-A1-S}$, (c) $FBG_{GS-A2-C}$, (d) $FBG_{GS-A2-S}$, (e) $FBG_{GS-A3-C}$, and (f) $FBG_{GS-A3-S}$.

Table 3 Comparison of experimental and theoretical values of test specimens（K_{T-F} and K_{T-M}）with the temperature sensitivity coefficient.

FBG number	K_{T-F} experimental value ($\times10^{-2}$ nm/℃)	K_{T-F} theoretical value (10^{-2} nm/℃)	K_{T-F} error rate between experimental and theoretical values (%)	K_{T-M} experimental value ($\times10^{-2}$ nm/℃)	K_{T-M} theoretical value ($\times10^{-2}$ nm/℃)	K_{T-M} error rate between experimental and theoretical values (%)	$K_{T-M}-K_{T-F}$ experimental value ($\times10^{-2}$ nm/℃)	$K_{T-M}-K_{T-F}$ theoretical value ($\times10^{-2}$ nm/℃)	$K_{T-M}-K_{T-F}$ error rate between experimental and theoretical values (%)
$FBG_{SW-A1-C}$	1.086	1.088	–0.184	2.450	2.451	–0.001	1.364	1.363	0.734
$FBG_{SW-A1-S}$	1.090	1.088	0.184	2.456	2.451	0.204	1.366	1.363	0.220
$FBG_{SW-B1-C}$	1.075	1.088	–1.195	2.446	2.451	–0.204	1.371	1.363	0.587
$FBG_{SW-B1-S}$	1.093	1.088	0.460	2.440	2.451	–0.449	1.347	1.363	–1.174
$FBG_{SW-A2-C}$	1.065	1.093	–2.562	2.441	2.464	–0.933	1.376	1.371	0.365
$FBG_{SW-A2-S}$	1.082	1.093	–1.006	2.451	2.464	–0.528	1.369	1.371	–0.146
$FBG_{SW-B2-C}$	1.093	1.093	0.000	2.464	2.464	0.000	1.371	1.371	0.000
$FBG_{SW-B2-S}$	1.091	1.093	–0.183	2.471	2.464	0.284	1.38	1.371	0.656
$FBG_{SW-A3-C}$	1.105	1.099	0.546	2.462	2.477	–0.606	1.357	1.378	–1.524
$FBG_{SW-A3-S}$	1.092	1.099	–0.637	2.446	2.477	–1.252	1.354	1.378	–1.742
$FBG_{SW-B3-C}$	1.103	1.099	0.364	2.445	2.477	–1.292	1.342	1.378	–2.612
$FBG_{SW-B3-S}$	1.095	1.099	–0.364	2.461	2.477	–0.646	1.366	1.378	–0.871
$FBG_{CFRP-A1-C}$	1.101	1.088	1.195	1.865	1.869	–0.214	0.764	0.781	–2.177
$FBG_{CFRP-A1-S}$	1.093	1.088	0.460	1.860	1.869	–0.482	0.767	0.781	–1.793
$FBG_{CFRP-B1-C}$	1.094	1.088	0.551	1.870	1.869	0.054	0.776	0.781	–0.640
$FBG_{CFRP-B1-S}$	1.106	1.088	1.654	1.880	1.869	0.589	0.774	0.781	–0.896
$FBG_{CFRP-A2-C}$	1.098	1.093	0.457	1.876	1.879	–0.160	0.778	0.786	–1.018
$FBG_{CFRP-A2-S}$	1.095	1.093	0.183	1.875	1.879	–0.213	0.78	0.786	–0.763
$FBG_{CFRP-B2-C}$	1.093	1.093	0.000	1.869	1.879	–0.532	0.776	0.786	–1.272
$FBG_{CFRP-B2-S}$	1.089	1.093	–0.366	1.869	1.879	–0.532	0.780	0.786	–0.763
$FBG_{CFRP-A3-C}$	1.105	1.099	0.546	1.879	1.889	–0.529	0.774	0.790	–2.025
$FBG_{CFRP-A3-S}$	1.104	1.099	0.455	1.890	1.889	0.053	0.786	0.790	–0.506
$FBG_{CFRP-B3-S}$	1.103	1.099	0.364	1.890	1.889	0.053	0.787	0.790	–0.380
$FBG_{CFRP-B3-C}$	1.094	1.099	–0.455	1.888	1.889	–0.053	0.794	0.790	0.506
$FBG_{FGRP-A1-C}$	1.075	1.088	–1.195	1.620	1.619	0.062	0.545	0.531	2.637
$FBG_{FGRP-A1-S}$	1.083	1.088	–0.460	1.623	1.619	0.247	0.540	0.531	1.695
$FBG_{FGRP-B1-C}$	1.085	1.088	–0.276	1.625	1.619	0.371	0.540	0.531	1.695
$FBG_{FGRP-B1-S}$	1.089	1.088	0.092	1.623	1.619	0.247	0.534	0.531	0.565
$FBG_{FGRP-A2-C}$	1.080	1.093	–1.189	1.626	1.628	–0.123	0.546	0.535	2.056
$FBG_{FGRP-A2-S}$	1.083	1.093	–0.915	1.612	1.628	–0.983	0.529	0.535	–1.121
$FBG_{FGRP-B2-C}$	1.093	1.093	0.000	1.631	1.628	0.184	0.538	0.535	0.561
$FBG_{FGRP-B2-S}$	1.088	1.093	–0.457	1.636	1.628	0.491	0.548	0.535	2.430
$FBG_{FGRP-A3-C}$	1.105	1.099	0.546	1.642	1.636	0.367	0.537	0.537	0.000
$FBG_{FGRP-A3-S}$	1.090	1.099	–0.819	1.632	1.636	–0.244	0.542	0.537	0.931
$FBG_{FGRP-B3-C}$	1.098	1.099	–0.091	1.633	1.636	–0.183	0.535	0.537	–0.372
$FBG_{FGRP-B3-S}$	1.094	1.099	–0.455	1.635	1.636	–0.061	0.541	0.537	0.745

3.3 Test of the FBG strain sensitivity coefficient $K_{\varepsilon-M}$ of coupling substrates

Strain sensitivity coefficients $K_{\varepsilon-M}$ of the FBG sensors were measured by adopting the stepped tensioning of members with coupling FBG sensors on the tensioning pedestal. The schematic diagram of the tensioning pedestal is shown in Fig. 4. Tensioning includes two steps: pre-tensioning and formal tensioning. Pre-tensioning: (1) 0.2 Pn pre-tensioning was performed on members and then decreased to 0.05 Pn; (2) 0.1 Pn tensioning per step from 0.05 Pn at the speed of no more than 100 MPa/min was performed, and the readings of the grating demodulator and stress and the readings of the dial gauge were recorded after sustaining load for 5 min; (3) stepped tensioning was 0.35 Pn which sustained the load for 10 min; (4) the load was decreased to 0.05 Pn; (5) repeated steps (2) to (4), namely tensioning unloading, as shown in Fig. 5. Formal tensioning: the load was increased from 0.05Pn until it reached the 0.65Pn，taking 0.1Pn as the load of each step. After holding the load for 5 minutes at each step, the readings of the grating demodulator, stress, and dial gauge were recorded at the same time, as shown in Fig. 6. Pn is the ultimate load-carrying capacity of specimens, where Pn of the steel wire was 39.5 kN, Pn of the carbon fiber substrate was 62.2 kN, and Pn of the fiberglass reinforcement substrate was 17.2 kN.

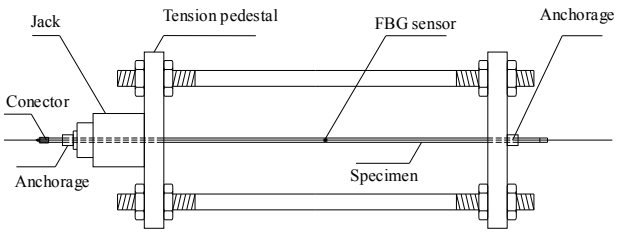

Fig. 4 Schematic diagram of the tensioning pedestal.

Linear fitting was achieved with variations of the FBG central wavelength $\Delta\lambda_B$ as the ordinate and the strain of the specimen as the abscissa. The carbon fiber substrate was taken as an example which is shown in Fig. 6. For the strain of specimen $\varepsilon_m = F/EA$, F is the tensioning stress, E is the elastic modulus of a specimen, and A is the cross-sectional area of the specimen. As shown in Fig. 7, the fitting of Groups A and B almost coincides with each other, which suggests that the use of the preloading technique and non-preloading technique has no impact on the strain sensitivity coefficients of the FBG coupled with substrates.

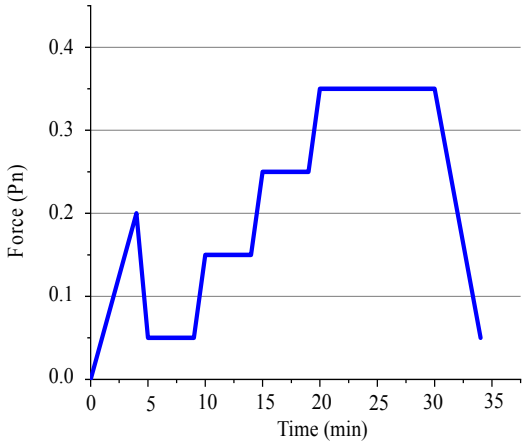

Fig. 5 Pretension profile of the specimens.

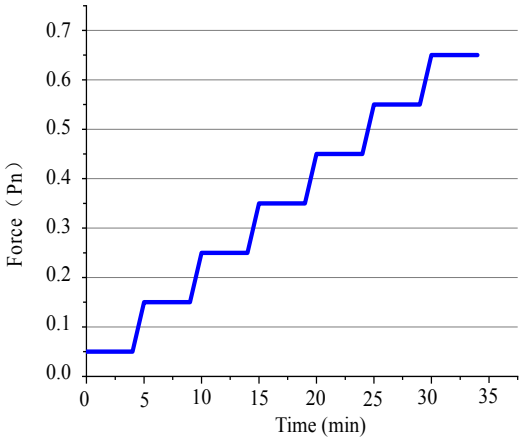

Fig. 6 Pretension profile of the specimens.

The theoretical strain sensitivity coefficients of the FBG embedded onto substrates can be simulated as

$$K_{\varepsilon-M} = (1 - P_e)\lambda_B . \quad (8)$$

The experimentally observed (test data) and theoretical values are comparatively listed in Table 4.

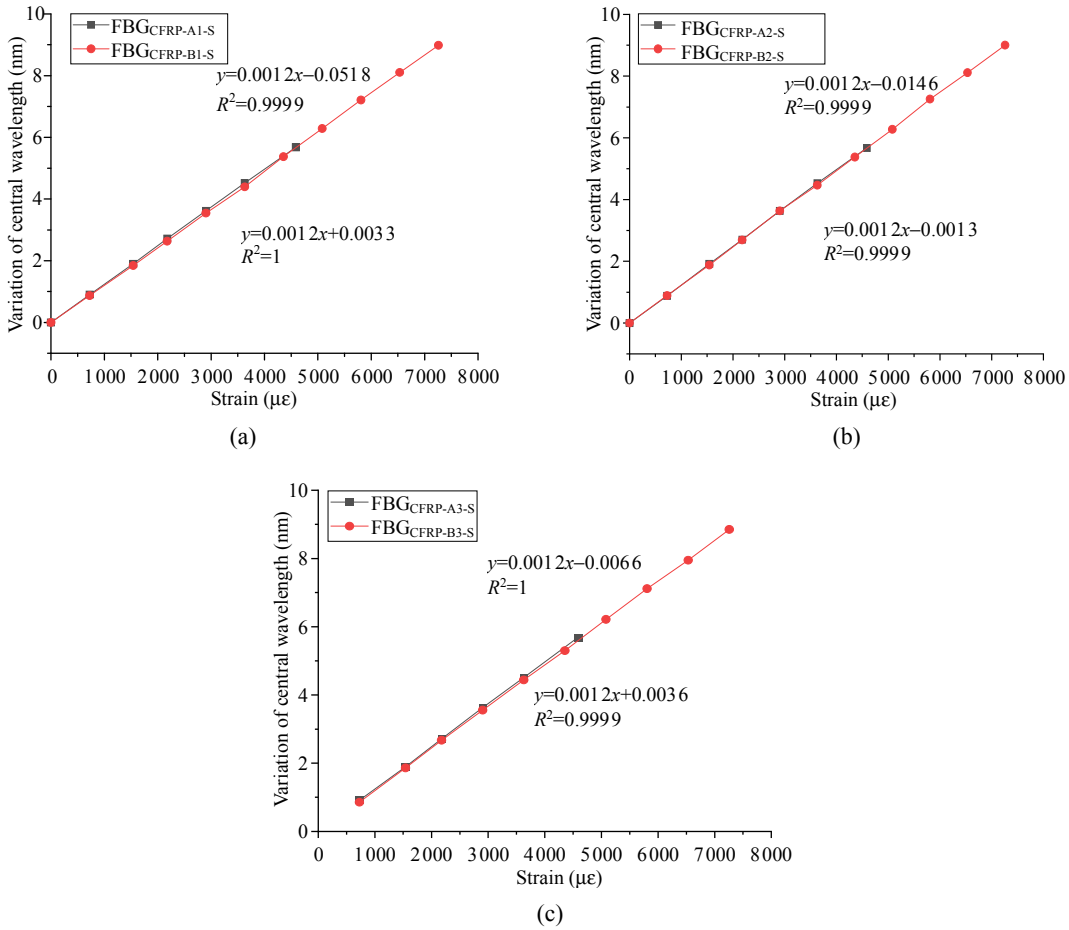

Fig. 7 FBG strain sensitivity coefficient $K_{\varepsilon-M}$ of the carbon fiber substrate: (a) FBG$_{CFRP-A1-S}$, FBG$_{CFRP-B1-S}$, (b) FBG$_{CFRP-A2-S}$, FBG$_{CFRP-B2-S}$, and (c) FBG$_{CFRP-A3-S}$, FBG$_{CFRP-B3-S}$.

Table 4 Comparison between experimental and theoretical values of the strain sensitivity coefficient $K_{\varepsilon-M}$.

FBG number	Experimental value $K_{\varepsilon-M}$ ($\times10^{-3}$ nm / με)	$K_{\varepsilon-M}$ calculated by (8) ($\times10^{-3}$ nm / με)	Error rate between experimental and theoretical values (%)
FBG$_{SW-A1-S}$	1.201	1.195	0.502
FBG$_{SW-B1-S}$	1.200	1.195	0.418
FBG$_{SW-A2-S}$	1.199	1.201	–0.167
FBG$_{SW-B2-S}$	1.198	1.201	–0.250
FBG$_{SW-A3-S}$	1.197	1.207	–0.829
FBG$_{SW-B3-S}$	1.210	1.207	0.249
FBG$_{CFRP-A1-S}$	1.191	1.195	–0.335
FBG$_{CFRP-B1-S}$	1.200	1.195	0.418
FBG$_{CFRP-A2-S}$	1.205	1.201	0.333
FBG$_{CFRP-B2-S}$	1.210	1.201	0.749
FBG$_{CFRP-A3-S}$	1.199	1.207	–0.663
FBG$_{CFRP-B3-S}$	1.205	1.207	–0.331
FBG$_{FGRP-A1-S}$	1.190	1.195	–0.418
FBG$_{FGRP-B1-S}$	1.194	1.195	–0.084
FBG$_{FGRP-A2-S}$	1.211	1.201	0.833
FBG$_{FGRP-B2-S}$	1.199	1.201	–0.167
FBG$_{FGRP-A3-S}$	1.215	1.207	0.663
FBG$_{FGRP-B3-S}$	1.210	1.207	0.249

Notes: Strain sensitivity coefficients of the temperature compensation FBG were not required in this test, so only the strain sensitivity coefficients of the strain FBG were measured.

The comparative analysis of the data in Table 4 leads us to predict that the test and theoretical values of the FBG sensor strain sensitivity coefficients $K_{\varepsilon-M}$ in these three substrates have similar results with an error rate of less than 1%. It showed that the embedded preloading process could realize the synchronous strain between the substrate material and the optical fiber. This result was consistent with that of our previous work where the strain transfer rate could reach 0.978 [26]. The CTE of the substrate materials and preloading technique did not affect $K_{\varepsilon-M}$. According to the theoretical formula $K_{\varepsilon-M}=(1-P_e)\lambda_B$, the strain sensitivity coefficients were due to the FBG, which was only related to its elastic-optical coefficient and initial central wavelength.

4. Temperature compensation test

4.1 Test device

In order to perform a test in the designed device, the substrates coupled with the FBG strain sensors were loaded through prestressing tensioning pedestal and four alcohol lamps were used for uniform heating in the glass tube where the strain grating was located. One of the alcohol lamps was used for heating in the glass tube where the temperature compensation grating was located so that the two gratings could be synchronously heated. An electronic thermometer with an accuracy of 0.1 ℃ was inserted into the end of the glass tube and sealed with the sealant. A schematic diagram of the temperature compensation test device is shown in Fig. 8. The FBG between the tensioning pedestals was the strain FBG which was affected by both strain and temperature variations, while the FBG outside the anchorage was the temperature compensation FBG sensor, which was only affected by temperature.

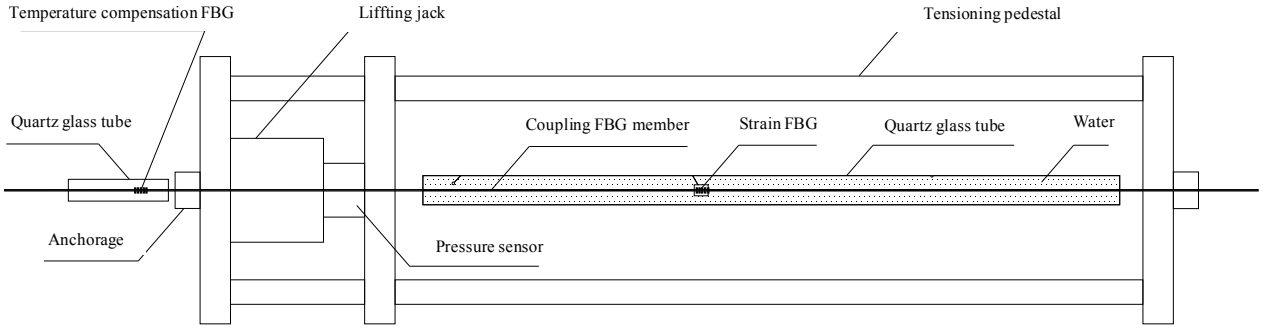

Fig. 8 Schematic diagram of temperature compensation test device.

The data of the test specimen are listed in Table 2. The substrate materials embedded with the FBG were put through the tensioning pedestal and quartz glass tube with the strain FBG between the two anchorages. Besides, the temperature compensated FBG was embedded with the substrate material which was the same as the substrate material embedded with the strain FBG and the substrate material embedded with the temperature compensated FBG outside the anchored ends, namely temperature compensation with one free end, as shown in Fig. 8. The specimen was anchored by the anchorage on the tensioning pedestal. The glass tube filled with water was sealed from two ends and the temperature change during heating was recorded by the temperature gauge. The initial temperature was 30 ℃ which was increased to 100 ℃ with 10 ℃ per step under a certain tensioning sustaining load. The strain FBG and temperature compensation sensors were collected when the temperature at each step remained stable. The tensioning anchoring stress was 0.3 Pn (Pn was the ultimate load-carrying capacity of the specimen). The test device is shown in Fig. 9.

Fig. 9 Test device.

The linear fitting has been achieved from the data of temperature compensation FBG sensors along with variations of the central wavelength of the temperature compensation FBG $\Delta\lambda_B$ as the ordinate and temperature T as the abscissa. The resulting temperature sensitivity coefficients K_{T-M-C} of the temperature compensation FBG are compared with those of specimens with two free ends, and the data are shown in Table 5.

Table 5 Comparison of experimental data (K_{T-M-C} and K_{T-M}) for one free end and two free ends.

FBG number	K_{T-M-C} experimental value ($\times10^{-2}$ nm/℃)	K_{T-M} experimental value ($\times10^{-2}$ nm/℃)	Error of temperature sensitivity coefficient of one end free K_{T-M-C} and two ends free K_{T-M} (%)
$FBG_{SW-A1-C}$	2.444	2.450	0.25
$FBG_{SW-B1-C}$	2.457	2.446	0.45
$FBG_{SW-A2-C}$	2.450	2.441	0.37
$FBG_{SW-B2-C}$	2.477	2.464	0.52
$FBG_{SW-A3-C}$	2.459	2.462	–0.12
$FBG_{SW-B3-C}$	2.438	2.445	–0.29
$FBG_{CFRP-A1-C}$	1.852	1.865	0.70
$FBG_{CFRP-B1-C}$	1.865	1.870	–0.27
$FBG_{CFRP-A2-C}$	1.867	1.876	–0.48
$FBG_{CFRP-B2-C}$	1.875	1.869	0.32
$FBG_{CFRP-A3-C}$	1.890	1.879	0.58
$FBG_{CFRP-B3-C}$	1.875	1.888	–0.69
$FBG_{FGRP-A1-C}$	1.634	1.620	0.86
$FBG_{FGRP-B1-C}$	1.635	1.625	0.61
$FBG_{FGRP-A2-C}$	1.616	1.626	–0.62
$FBG_{FGRP-B2-C}$	1.628	1.631	–0.18
$FBG_{FGRP-A3-C}$	1.652	1.642	0.61
$FBG_{FGRP-B3-C}$	1.643	1.633	0.61

As can be analyzed from the data of Table 5, temperature sensitivity coefficients of the temperature compensation FBG sensor in two states are almost the same, with an error rate of less than 1%. This indicates that the end restraint does not affect the temperature sensitivity coefficients of FBG sensors.

Temperature sensitivity coefficients K_{T-M-C} of the temperature compensation FBG sensor, temperature sensitivity coefficients K_{T-M-S}, strain sensitivity coefficients $K_{\varepsilon-M-S}$ of the strain FBG(data in Tables 3 and 4 adopted), and the variations of the central wavelength of the temperature compensation FBG and the strain FBG $\Delta\lambda_C$ and $\Delta\lambda_S$ were recorded. These were monitored along with an increase in the temperature per step, using (7), and the strain (ε) of the specimen was calculated. The strain was taken as the ordinate, and the temperature was taken as the abscissa. The comparative strain values, measured by the electronic dynamometer using (7) with the strain values obtained after the temperature compensation are shown in Fig. 10.

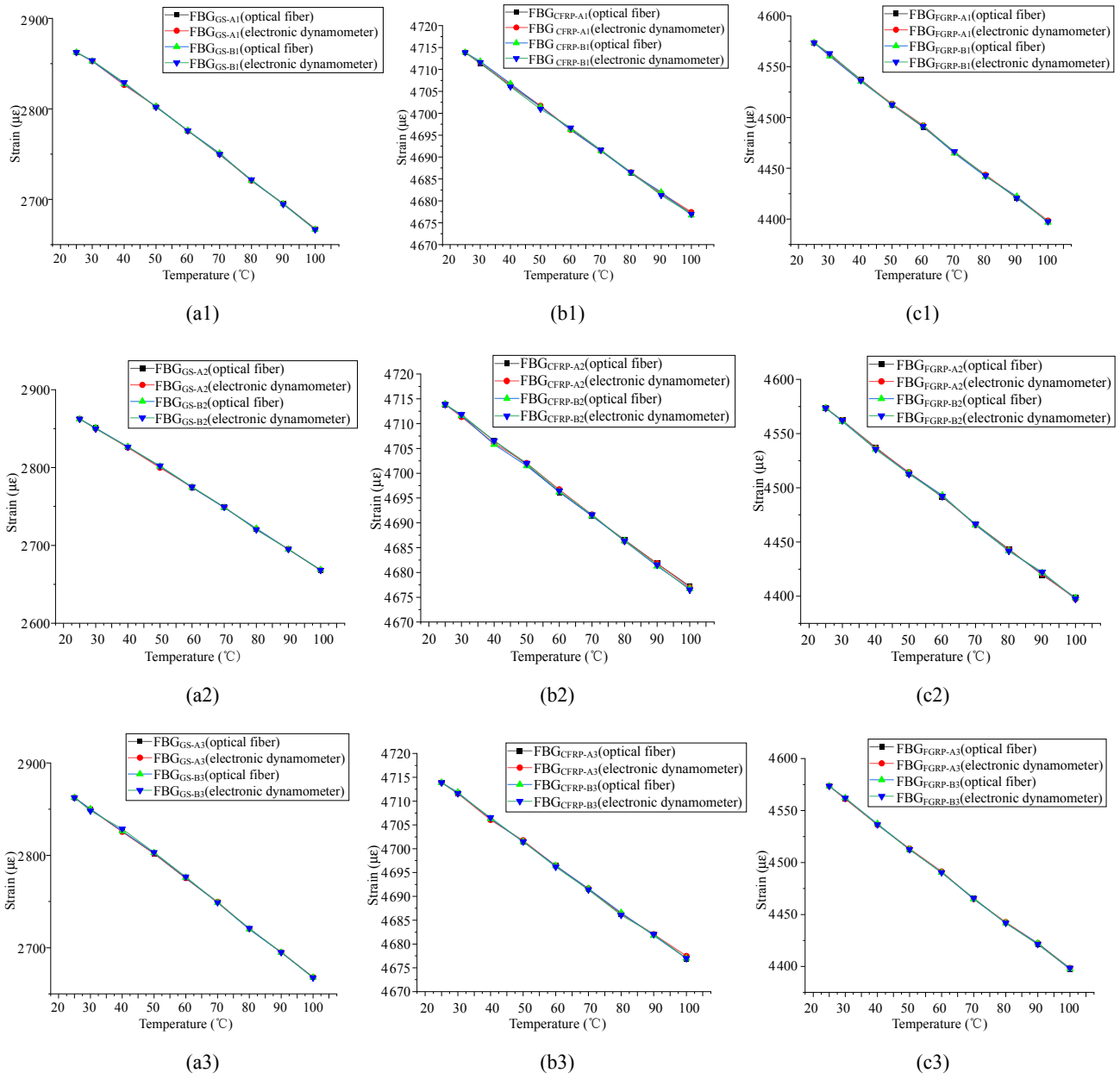

Fig. 10 Comparison between the strain value obtained after temperature compensation of the corresponding variable grating and the strain value measured by the electronic dynamometer: (a1) FBG_{GS-A1} and FBG_{GS-B1}, (a2) FBG_{GS-A2} and FBG_{GS-B2}, (a3) FBG_{GS-A3} and FBG_{GS-B3}, (b1) $FBG_{CFRP-A1}$ and $FBG_{CFRP-B1}$, (b2) $FBG_{CFRP-A2}$ and $FBG_{CFRP-B2}$, (b3) $FBG_{CFRP-A3}$ and $FBG_{CFRP-B3}$, (c1) $FBG_{FGRP-A1}$ and $FBG_{FGRP-B1}$, (c2) $FBG_{FGRP-A2}$ and $FBG_{FGRP-B2}$, and (c3) $FBG_{FGRP-A3}$ and $FBG_{FGRP-B3}$.

Note: the optical fiber in the figure is the strain value measured by the embedded fiber grating, and the electronic dynamometer is the strain value measured by the electronic dynamometer.

As shown in Fig. 10, the temperature variations have a negative correlation along with the variations of the strain. The higher the temperature is, the smaller the tensioning strain is. The reason behind this is that the higher temperature leads to an increase in the strain, thus reducing the tensioning strain. This statement is also consistent with an actual decrease in the anchoring strain of the bridge cable with an increase in the temperature. In Fig. 10, the strain value was calculated from (7) which was measured by a pressure sensor. This showed the maximum difference of 2.65 με with an error rate of less than 1%. So, this could be almost ignored in the actual engineering. It was proven that this

method of the temperature compensation had a high accuracy.

Considering one substrate, different FBG central wavelengths had nearly no effect on the monitored result or temperature compensation as can be seen in Fig. 10. For the specimens in Groups A and B with the same FBG central wavelength, their fitting curves were almost overlapped. This overlap suggested that the preloading and non-preloading coupling techniques had no impact on the performance of the temperature compensation.

Stressing states of different substrate materials are compared in Fig. 11. The larger the expansion coefficient of substrate materials is, the faster the reduction of the tensioning stress will be along with an increase in the temperature.

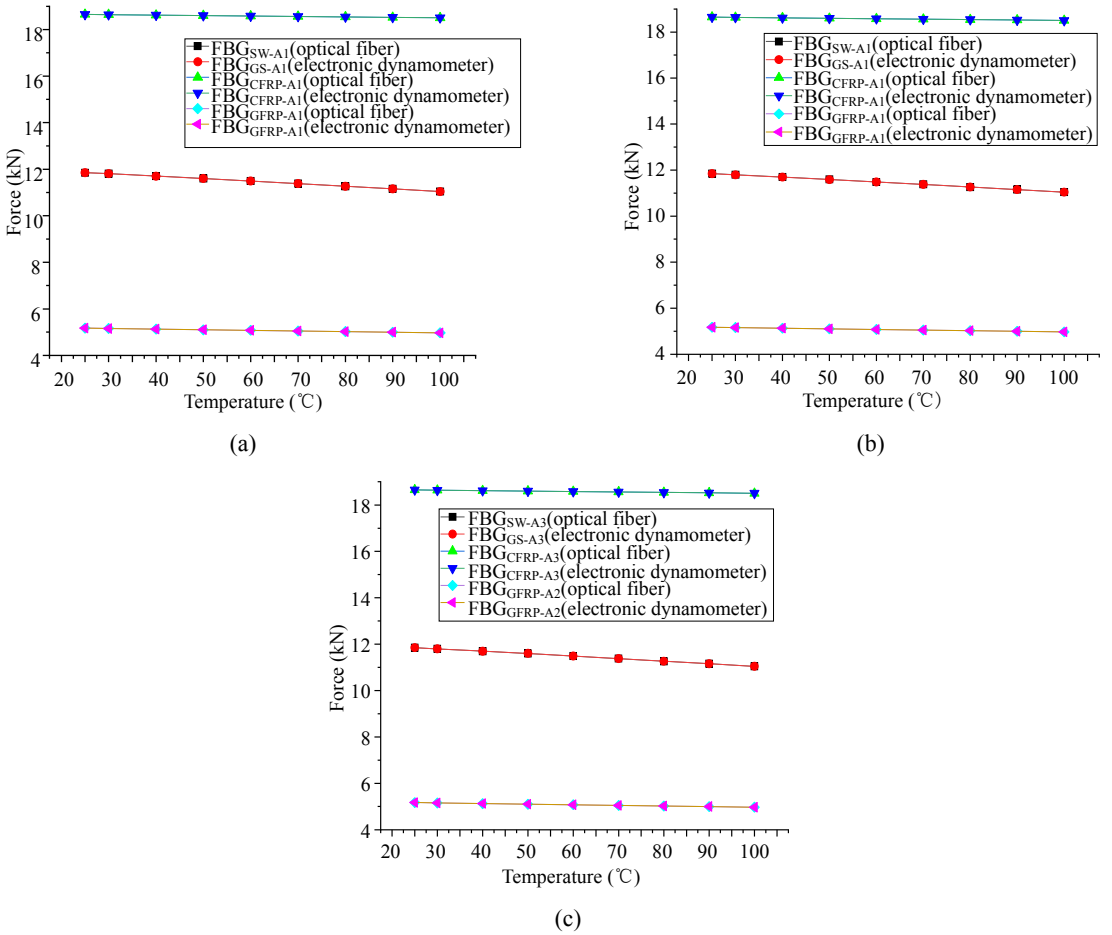

Fig. 11 Comparison of stress monitoring after the FBG temperature compensation of different substrate materials: (a) 1532 nm, (b) 1540 nm, and (c) 1548 nm.

In terms of Fig. 11, the fitting curves of stress data were measured by the FBG and gained from the pressure sensor almost overlapped, as can be seen in Fig. 11. This indicated the high accuracy of (7) for monitoring the FBG strain, caused by the temperature compensation.

5. Conclusions

In this paper, comprehensive theoretical and experimental studies have been conducted on the strain-temperature cross-sensitivity of the FBG strain sensors on different substrates. A series of cross-sensitivity tests were designed, and the tests were systematically performed based on the temperature compensation reference grating method. This laid a foundation for engineering applications in strain monitoring of components, embedded with the FBG sensors. The main points of this work were

as follows:

(1) Using the temperature compensation grating method, the strain-temperature cross-sensitivity problem of the FBG strain sensor was theoretically studied and the theoretical formula of the temperature compensation was derived. In the experimental test, the fitting of the stress value was calculated as the formula and measured by a pressure sensor. These were almost overlapped which suggested the high accuracy of this temperature compensation method.

(2) In the case of the temperature compensation FBG or strain FBG, both the theoretical and experimental data of temperature sensitivity coefficients and strain sensitivity coefficients had some errors. In order to consider the actual engineering aspects, the sensitivity coefficients should be measured by the calibration method instead of directly using the theoretical values.

(3) When the FBG sensors were coupled with different substrates, their temperature sensitivity coefficients were quite different from those of the bare FBG, which were directly related to the CTEs of substrates. Therefore, when the temperature compensation reference grating method was applied, the temperature compensation FBG should be coupled with the same substrate material with monitoring strain FBG and then calibrated together. Rather than the temperature sensitivity, the coefficients of the bare FBG or FBG with different substrate materials were adopted.

(4) Three different kinds of FBG central wavelengths had almost no impact on the monitored result and temperature compensation. So, the temperature compensation FBG could be used with a central wavelength similar to that of monitoring strain FBG.

(5) While considering the temperature compensation FBG with one or two free ends in the specimens test, their temperature sensitivity coefficients were almost the same. So, the temperature compensation FBG could be set on the end outside the anchoring part of members in engineering applications. And the temperature compensation FBG had the same substrate material, but both should have a similar variation field of temperature.

(6) The preloading and non-preloading techniques had almost no impact on the temperature compensation. The FBG monitoring range was sufficient for the temperature variations of –50 ℃ and 100 ℃. So, to simplify the technique process, the preloading technique was not required in the temperature compensation FBG.

Acknowledgment

This work was supported by the National Natural Science Foundation of China (Grant No. 52068014); Key Research & Development Projects in the Guangxi Autonomous Region (Grant No. GUIKE AA20302006); Major Construction Program of the Science and Technological Innovation Base in the Guangxi Autonomous Region (Grant No. 2018-242-G02). And authors would like to express their gratitude to EditSprings (https://www.editsprings.cn) for the expert linguistic services provided.

References

[1] G. W. Yao, X. R. Yu, L. F. Gu, and Y. X. Jiang, “Experiment on corrosion fatigue life of steel strands under the coupling effects of chloride environment and alternating loads,” *Advances in Civil Engineering*, 2021, 2021(Pt.1): 2439503.

[2] P. Wang, L. Zhang, F. M. Wang, Z. P. Zhang, and Y. He, “The time-dependent effect of corrosion of steel strands on prestressed concrete beam bridges,” *Applied Mechanics and Materials*, 2014, 638: 1038–1044.

[3] C. Lan, Y. Xu, C. Liu, H. Li, and B. F. Spencer Jr, "Fatigue life prediction for parallel-wire stay cables considering corrosion effects," *International Journal of Fatigue*, 2018, 114: 81–91.
[4] Z. Liu, Q. Huang, Y. Shan, and J. Chen, "Quantifying high temperature – induced breakage instant of prestressing high-strength steel wire," *Journal of Materials in Civil Engineering*, 2020, 32(7): 04020189.
[5] C. M. Lan, H. T. Yang, N. N. Bai, and C. P. Liu, "Probabilistic model for fatigue life evaluation of corroded prestressing strand," *China Civil Engineering Journal*, 2018, 51(10): 68–77.
[6] S. L. Huang, B. Q. Tao, and Y. P. Shen, "Intelligent structure systems: dream, reality, and future," in *World Forum on Smart Materials & Smart Structures*, China, 2007, pp. 22–27.
[7] J. M. W. Brownjohn, "Structural health monitoring of civil infrastructure," *Philosophical Transactions Mathematical Physical & Engineering Sciences*, 2007, 365(1851): 589–622.
[8] J. P. Ou, "Monitoring and maintenance of large bridge life cycle performance," *China Highway*, 2017, 13: 42–45.
[9] L. M. Sun, Z. Q. Shang, and Y. Xia, "Development and prospect of bridge structural health monitoring in the context of big data," *China Journal of Highway and Transport*, 2019, 32(11): 1–20.
[10] J. M. Kim, H. W. Kim, S. Y. Choi, and S. Y. Park, "Measurement of prestressing force in pretensioned UHPC deck using a fiber optic FBG sensor embedded in a 7-wire strand," *Journal of Sensors*, 2016, (2016): 1–9.
[11] X. Kong, J. Zhang, L. Deng, and Y. K. Liu, "Research advances on vehicle parameter identification based on machine vision," *China Journal of Highway and Transport*, 2021, 34(4): 13.
[12] D. Li, Z. Zhou, and J. P. Ou, "Dynamic behavior monitoring and damage evaluation for arch bridge suspender using GFRP optical fiber Bragg grating sensors," *Optics & Laser Technology*, 2012, 44(4): 1031–1038.
[13] C. B. Xiong, H. L. Lu, J. S. Zhu, and J. Y. Yu, "Dynamic deformation monitoring of bridge structures based on GPS-RTK and accelerometers," *Journal of Vibration and Shock*, 2019, 38(12): 69–73.
[14] C. Lan, Z. Zhou, and J. P. Ou, "Monitoring of structural prestress loss in RC beams by inner distributed Brillouin and fiber Bragg grating sensors on a single optical fiber," *Structural Control and Health Monitoring*, 2014, 21(3): 317–330.
[15] J. M. Kim, C. M. Kim, S. Y. Choi, and B. Y. Lee, "Enhanced strain measurement range of an FBG sensor embedded in seven-wire steel strands," *Sensors (Basel, Switzerland)*, 2017, 17(7): 1654.
[16] W. X. Zhu, H. Y. Qin, J. Z. Li, and J. P. Ou, "Monitoring cable force of FAST project based on fiber Bragg grating sensor external installed on anchorage zone," *Journal of Mechanical Engineering*, 2017, 53(17): 23–30.
[17] T. Shiratsuchi and T. Imai, "Development of fiber Bragg grating strain sensor with temperature compensation for measurement of cryogenic structures," *Cryogenics*, 2021, 113: 103233.
[18] H. P. Wang, J. G. Dai, and X. Z. Wang, "Improved temperature compensation of fiber Bragg grating-based sensors applied to structures under different loading conditions," *Optical Fiber Technology*, 2021, 63: 102506.
[19] J. F. Wang, Y. Yu, Y. Chen. H. Luo, and Z. Meng, "Research of a double fiber Bragg gratings vibration sensor with temperature and cross axis insensitive," *Optik – International Journal for Light and Electron Optics*, 2015, 126(7–8): 749–753.
[20] T. Iwashima, A. Inoue, M. Shigematsu, M. Nishimura, and Y. Hattori, "Temperature compensation technique for fiber Bragg gratings using liquid crystalline polymer tubes," *Electronics Letters*, 1997, 33(5): 417–419.
[21] Y. S. Wang, Z. Q. Wang, T. Wang, and D. W. He, "A novel temperature self-compensation FBG vibration sensor," *Journal of Physics: Conference Series*, 2011, 276(1): 012146.
[22] M. F. Liang. "A fiber Bragg grating pressure sensor with temperature compensation based on diaphragm-cantilever structure," *Optik*, 2017, 145: 503–512.
[23] Y. Huang, J. Li, G. Kai, S. Yuan, and X. Dong, "Temperature compensation package for fiber Bragg gratings," *Microwave and Optical Technology Letters*, 2003, 39(1): 70–72.
[24] Y. Kaung, Y. X. Guo, L. Xiong, and W. L. Liu, "Packaging and temperature compensation of fiber Bragg grating for strain sensing: a survey," *Photonic Sensors*, 2018, 8(4): 320–331.
[25] H. Y. Qin, W. X. Zhu, H. L. Zhang, Z. Zhou, and J. Ou, "Manufacturing and performance analysis of intelligent steel strand embedded with prepressure large scale fiber Bragg grating sensor," *Chinese Journal of Lasers*, 2017, 44(4): 0410001.
[26] H. Y. Qin, Q. X. Shen, W. X. Zhu, and H. L. Zhang, "Range-expansion technology and fatigue performance study on the self-sensing steel strand with an embedded fibre Bragg grating sensor," *Strain*, 2020, 56(5): e12354.
[27] H. Y. Qin, Q. X. Shen, J. P. Ou, and W. X. Zhu, "Long-term monitoring reliability and life prediction of fiber Bragg grating-based self-sensing steel strands," *Advances in Civil Engineering*, 2020(2020): 7687039.
[28] W. X. Zhu, Q. X. Shen, and H. Y. Qin, "Research

and application of FBG monitoring technology in internal prestressed steel strand," *Acta Photonica Sinica*, 2019, 48(2): 0206002.

[29] W. X. Zhu, Q. X. Shen, and H. Y. Qin, "Monitoring of prestress and bond stress of self-sensing FBG steel strand," *Measurement*, 2021(177): 109246.

[30] M. C. Wu, R. H. Pater, and S. L. DeHaven, "Effects of coating and diametric load on fiber Bragg gratings as cryogenic temperature sensors," *Proceedings of SPIE – The International Society for Optics and Photonics*, 2008, 6933: 28–37.

[31] H. Y. Qin and W. Q. Wan, "Temperature characteristics of fiber Bragg grating strain sensor with groove embedded package," *Railway Engineering*, 2020, 60(9): 57–59.